Chapter 4

Disorder processes in $A^{3+}B^{3+}O_3$ compounds: implications for radiation tolerance.

The work presented in this Chapter has been published in Philosophical Magazine [164].

4.1 Introduction

4.1.1 Motivation

The radiation tolerance of perovskite phases is of importance since (Ca,Sr)TiO_3 compositions are a constituent of the Synroc nuclear waste package. Experimental studies have deduced that these phases undergo cation disorder leading to amor-

phisation. This in turn causes rapid leaching of radionuclides into the environment. One root of this amorphisation is the self irradiation of the ceramic by the decay of radionuclides. Cation disorder in particular induces lattice strain, due to the cation size mismatch of an A^{2+} cation on a B^{4+} site (and vice versa), but also the charge variance. The work presented in this chapter investigates the radiation tolerance of an array of perovskite compositions, where both the A and B cations adopt a 3+ valance state, by comparing the energies of the intrinsic defect processes as a function of composition. This allows for the identification of compositions that will be tolerant to intrinsic disorder processes. The initial sections of this chapter give an overview of issues and background relating to nuclear waste disposal and the radiation tolerance of ceramic materials. The results are then presented and comparisons drawn with the radiation tolerance of pyrochlore materials which have previously been investigated using the same computational approach.

4.1.2 Radioactive Waste

The 1940s and 1950s were the formative years of the nuclear industry. This was initiated by an arms race, first between the Allies and the Axis during the Second World War and then between the West[1] and the Soviet Block during the Cold-War. There was a massive drive to at first create (via the Manhattan project) and then to develop increasingly powerful nuclear weapons. The rush to attain these goals meant that insufficient attention was given to radioactive waste management and led to the use of rather basic storage disposal facilities. This is illustrated by a consideration of the economics, e.g. the US spent billions of dollars to develop nuclear weapons

[1]The West is an ideological and political distinction between nations and generally refers to western Europe and the US [165].

and commercialize nuclear power during the 1950s and 1960s whilst only spending a few hundred million to research disposal processes [166]. As such one of the major issues affecting modern society politically, socially and scientifically is radioactive waste management. In a recent white paper, the British government estimated the cost of dealing with the UK's nuclear legacy at £48 billion [167]. The clean-up cost in the US is currently costing $6 billion per year and is approximately the same as the entire US Environmental Protection Agency budget [166]. The US Department of Energy (DoE) currently estimates that $147 billion will be needed by 2070 in order to complete the clean-up [168].

The combined effect of dwindling fossil fuel supplies (estimates vary but are usually around 40 years [169, 170]), the requirement to reduce greenhouse gas emission (in line with the Kyoto protocol [171]), together with insufficient progress of renewable energy resources, leaves nuclear power generation as a highly viable energy source for the near future. As such, if anything, the volumes of radioactive waste are set to increase.

Many nuclear waste types exist, and each can be dealt with in a different manner. Nevertheless, wastes can be categorised as a being one of four types: very low, low, intermediate and high level (adapted from [167]):

Very Low Level Waste (VLLW) Hospital and general industrial waste with low activities. Proper management at the source allows disposal through conventional routes via landfill and incineration.

Low Level Waste (LLW) Hospital, research facility and general industrial waste. Principally lightly contaminated scrap such as metal, soil and clothing. Disposal is at authorised sites only.

Intermediate Level Waste (ILW) Principally from decommissioning, fuel reprocessing and reactor facilities including metal and organic materials. The heat generated is not sufficient to be of concern for storage or disposal facilities. There is currently no final management strategy for long term storage in some countries. In the UK, much of this type of waste is processed into a cementitious form contained in steel canisters.

High Level Waste (HLW) Principally from spent nuclear fuel reprocessing. The activity levels are sufficient to cause self heating of the waste to a level that causes problems for storage. As with ILW there is no final management strategy for dealing with HLW.

Since insufficient consideration was given to radioactive waste, very simple disposal techniques have historically been used. Historical disposal methods (such as those used in the UK) can lead to an inhomogeneous waste mixture. Therefore, part of the clean-up process involves examination and determination of the wastes currently in historical disposal sites [167]. Compounding the problem with historical repositories is their instability due to a build-up of explosive gases at the top of the vessel.

Ineffective stores were also used in other countries, for example in the United States at the Hanford complex [172]. Here the waste remains a significant problem despite attempts to clean up the site with schemes such as leaching the liquid waste into the soil. Since leakage and gas explosions are possible threats, the highly unstable nature of historical waste facilities has driven the development of more stable and easily managed waste forms with increased longevity [173].

Since the inception of nuclear waste management many schemes have been proposed for the long-term storage of HLW, including immobilisation in clay, encapsulation

in ceramics/glasses, land burial, dilution, geological emplacement, disposal in fault zones, ice and space and finally transmutation. Of these, separation of the most dangerous (long half life and highly radioactively toxic) followed by transmutation (the use of reactors to produce less radiotoxic products through fission) is one of the most promising approaches for dealing with the waste, yet currently, the technology is not sufficiently advanced for this to be a viable economic method for dealing with waste. Presently, modified reactors are used to generate the neutrons for the transmutation, however there is work both in the US and the UK on the use of powerful lasers to generate gamma rays to transmute atoms [174]. An example of current technology for transmutation is the fast breeder reactors which are able to transmutate actinides since an excess of neutrons is generated by the fission process, and these reactors then generate (*breed*) new fissile material (other fissile actinides) faster than it is consumed. However, such reactors are not used for waste management [175]. As a result, the current global consensus for the effective long-term disposal of radioactive waste is via encapsulation followed by geological emplacement.

Of the various types of waste, the most hazardous is HLW (including spent fuel) of which there are very large volumes; in the United States alone there are approximately 385,000 cubic metres [176] with a total activity of between 1.2 [176] and 1.6 billion Curies [97] (4.4×10^{19} to 5.9×10^{19} Bq). This waste comes from several sources: the reprocessing of spent fuel rods from nuclear power plants, the decommissioning of nuclear weapons, and the decommissioning of naval propulsion units [176]. The major issue with the disposal of HLW is the necessity to ensure that the radio-nuclides remain within the waste package, that is, they do not enter the environment. HLW may be contained in stainless steel drums and stored in specsially prepared underground repositories (further discussion of this multibarrier

concept can be found later in this Chapter). To minimize the hazards, it is currently international policy to fix the radioactive waste in a solid form before transportation.

Multi-barrier Concept

Due to the importance of preventing radiotoxic elements from entering the biosphere, one method of protection alone is insufficient. A multibarrier protocol has been developed whereby the waste is isolated from the environment via a number of different barriers [97]. Firstly the waste is encapsulated in a host matrix, either ceramic or glass. This is then placed into a metal canister such as a hermetically sealed steal container. This container is then surrounded in a metallic overpack of mild steel, pure or alloyed titanium, which acts as a protective coating for the canister during handling. In order to provide structural support against geological pressures, a sleave is added to protect the package during removal from the clean-up site. Separating the waste packages from each other and the bedrock is the backfill, this is a clay or quartz and aids heat and load transfer and compatibility of all the components in the repository. To facilitate conditioning of the groundwater, immobilisation of the radionuclides and improved compatibility, a buffer is added. Finally a filler is used to fill space between the components.

The multi-barrier disposal scheme is discussed in a technical report of the International Atomic Energy Agency [177], and by Hench [97] and Ewing *et al.* [176].

Geological Emplacement

The aim of geological emplacement is to shield humanity, and indeed the rest of the environment, from the harmful radiation emanating from the HLW by using rock

and sediment. The main principles of the emplacement strategy are reported by Ewing [178]:

1. The repository should be deep, permanent and long-term, and to utilise the radiation decrease, thermal output and toxicity as an advantage.
2. The geological history of the site is indicative of the future geological stability e.g. seismic events, indicating that the site be analysed fully before use.
3. The passive hydraulic and geochemical properties of the site must be key to the isolation e.g. depth of water table.

Many countries are planning on using geological emplacement for the storage of HLW, however, there remains a point of contention regarding the time of operation of the repositories. There are some that believe that the repositories should remain open, so that future generations with more advanced technologies have the opportunity to employ improved methods for dealing with the waste (such as transmutation). This open scheme also has the added benefit that should geological changes occur at the site, the waste can be moved. However, with an open repository, there is a continual financial burden necessary to protect the site from human intrusion, either accidental or malicious. The other choice is to seal the repository. This is favoured by those who believe that future generations should not have to manage our current nuclear legacy. Under this scheme, the repository should involve no human intervention, being sealed by backfilling [179]. The problem with the sealed approach is that suitable sites must be investigated more thoroughly since the timescales over which they should be geologically stable are immense. As such, the sites are investigated to the fullness that the current level of geological science allows, a process which is both time consuming and expensive.

There are currently two sites in the US that are under consideration for this purpose, the Waste Isolation Pilot Plant (WIPP) in New Mexico and the Yucca mountain site in Nevada [178, 180–182]. The WIPP is currently receiving transuranic wastes from defence programs [166, 178]. Characterisation of the Yucca mountain site began in 1987 [183]. Many agencies are involved in the testing of the site. For example the Environmental Protection Agency (EPA) has proposed radiation protection standards and the Nuclear Regulatory Commission (NRC) has proposed rules for implementing standards for disposal schemes. However, despite this gargantuan project, the Yucca mountain site will be unable to accept any HLW until at least 2020 [173].

Encapsulation

There has been many material types considered for the encapsulation of HLW including glasses, polyphase ceramics and concretes (see [97, 176, 184–188] for examples). On the basis of an extensive evaluation of the different waste forms, borosilicate glasses and titanate based polyphase ceramics were selected for further development in 1982 [97]. Borosilicate glass has several advantages over the polyphase ceramic waste forms. The processability of glass compared to ceramic is significant, for example the slurry-fed glass melter is a one step process. This involves a low-melting, non-radioactive glass powder being mixed with the radioactive slurry to form a homogeneous network with the radionuclei becoming trapped in the three dimensional glass network. Such a processing route causes large compositional variability, however here another benefit of the glass is seen in that the waste form is insensitive to such variations [97]. As described earlier, the waste form will be subject to heating due to the radioactive decay of the waste, and again, the thermal stability of the glass has been seen to be favourable. However, the relative economics of the glass

and ceramics waste forms is still under debate as the waste loading of the ceramic is three times that of the glass [97].

To enable the secure immobilisation of the radioactive ions, it is preferable that the ceramic material into which they are inserted shows a regular crystalline lattice with very low defect concentrations since this minimises the flux via low energy transport mechanism. When a material is subjected to radiation damage, a large number of defects (much higher than equilibrium) are formed and become "frozen" into the lattice [189]. If the defect energy is high, the radiation damage leaves a large residual (retained) energy in the lattice, and as this excess energy accumulates it eventually leads to lattice amorphisation. This condition is more significant for cation defects as their mobility in ceramics is poor, and therefore they are difficult to anneal out of the lattice. Since anion mobility is generally far higher the criteria are slightly different, the important defect processes for the recovery involve anions, most notably the anion Frenkel reaction. As such, a low retained cation energy is a necessary, but not complete condition for the radiation tolerance assessment of a material. Atomistic simulation can be used to investigate the radiation tolerance of crystalline oxides. For example, a recent study by Sickafus *et al.* [4] assessed the stability of pyrochlores (complex oxides with a fluorite-related structure) for application in HLW storage. They analysed the energy of the localized disorder, in this system, and assumed that cation disorder commenced via the anti-site reaction (Equation 4.5).

Several polyphase ceramic materials are currently being considered for the long-term encapsulation of the radioactive waste, with one of the more promising being Synroc or "synthetic rock" which was initially developed by Prof. Ted Ringwood of the Australian National University in 1978 [190,191]. Synroc is a mineral analogue that

was specifically designed to immobilise HLW and contains a series of highly durable titanate phases. There are several variants of Synroc that have been investigated for specific applications, for example, Synroc C was designed for the immobilization of liquid HLW from the reprocessing of light water reactor fuel [182]. The composition of Synroc mainly includes natural titanate materials such as zirconolite ($CaZrTi_2O_7$), hollandite ($BaAl_2Ti_6O_{16}$) and perovskite ($CaTiO_3$) [176]. Different transuranic elements are known to partition to the various phases within Synroc, e.g. neptunium (Np) will be incorporated into the zirconolite [184]. These waste elements incorporate into Synroc via a substitutional solid solution mechanism [184]. Within the Synroc phases, the elements substitute onto different lattice sites depending upon their relative ionic radii and valence. Consequently, the radiation tolerance of single perovskite phases has been investigated as part of an overall strategy to understand which of the Synroc phases are the most radiation tolerant.

Within Synroc, the low durability of the perovskite is masked by the high durability of other constituent phases [192]. The leaching of the waste elements from the perovskite phase increases with increasing damage to the crystal structure, which can be considerable - one study even found the formation of anatase (TiO_2) within a perovskite sample doped with Curium (Cm) [192].

Other schemes to immobilize the HLW are in development; one of the more promising is a Synroc-glass composite, which is being studied at the Australian Nuclear Science and Technology Organization (ANSTO), the French Atomic Energy commission and the Russian Ministry for Atomic Energy (Minatom) [182]. The reason for the interest in the Synroc-glass composite is the improved the relatively poor waste loading of the glass phase alone. The waste loading of the Synroc phase is much higher than that of the glass, Synroc-C, for example, can hold up to 30% HLW by weight [182].

Furthermore, so called vitreous waste forms often contain minor amounts of ceramic phase anyway.

Damage Types in Crystalline Materials

The radiation damage to the encapsulating matrix during disposal is relatively insignificant, yet, post-disposal radiation damage can be immense. It is estimated that the accumulated radiation dose at the end of 10,000 years is equivalent to 0.5 displacements per atom [176]. This is well within the range during which important changes in physical and chemical properties can occur, mainly the transition from a crystalline to amorphous state. When a material becomes irradiated, the energy imparted causes atomic disorder processes to occur. This disorder can lead to either swelling or, in some cases, contraction of the bulk material, which in turn causes the formation of microcracks. These microcracks are able to serve as fast migration pathways for the radioactive contaminants to escape the encasement.

It is possible for ionic materials to accommodate extensive disorder without exhibiting excessive structural deterioration. Disorder effects are mitigated to a large degree by the clustering and recombination of lattice defects during and subsequent to the irradiation bombardment. The associated lattice strains can also be accommodated by the simple relaxation of the neighbouring atoms or ions [193]. The majority of damage in ceramic materials is via elastic collisions, where nuclear particles collide with the atoms of the host lattice. If these incident particles have sufficient energy, the host atoms can become displaced, and these recoiling atoms are then able to collide with other lattice atoms causing further displacements. Given sufficient incident energy, such knock-on collisions can develop into significant collision cascades. If the radioactive particles are sufficiently fast and charged they can cause ionisation

of the host atoms so that charged defects such as excitons and polarons are formed. If nuclear reactions are induced by the incident particles, transmutation can occur whereby the unstable nuclei can radioactively decay to other atoms [193]. The alpha decay (release of a helium nucleus) of incorporated actinides causes the self damage in HLW forms and leads to a crystalline to amorphous transformation [188]. The degree to which the material becomes amorphous effects the leach rate of the HLW, and therefore the more damaged the host matrix becomes, the easier it is for the radionuclei to escape into the environment.

Perovskite Radiation Tolerance

The solid solution series of materials (Ca,Sr)TiO_3 are a component of the original compounds within Synroc [190] and as such, the majority of research concerning the radiation tolerance of perovskite materials has focused on such compositions. Waste elements are incorporated into each of the Synroc phases via a substitutional solid solution mechanism. The two phases capable of incorporating transuranic elements are zirconolite and perovskite [184]. Smaller radius ions (e.g. U^{4+}, Y^{3+} and Gd^{3+}) generally partition to zirconolite, while larger ions (e.g. Nd^{3+} and Ce^{3+}) partition to the perovskite [187]. The relative stability of the Synroc constituents upon exposure to leachants decreases from zirconolite to hollandite to perovskite [187]. Despite this, the average critical dose for the amorphisation for perovskite is 2 - 5 times higher than that for zirconolite [188].

When a perovskite is subjected to radiation damage, its cation sublattice will experience disorder, of which a common example is the antisite process, where A and B cations are "swapped". For materials such as (Ca,Sr)TiO_3, this introduces a major charge redistribution into the lattice with considerable associated strains. (This ef-

fect was first described by Zachariasen [194] for the example of metaboric acid where it was shown that an effective charge on a lattice site will cause a change in the bond lengths of the neighbouring oxygen ions). An additional factor contributing to the lattice strain associated with antisite disorder in perovskites is the significant size difference between the A and B cations.

Here studies of radiation tolerance in perovskites are extended by considering ABO_3 materials in which the A and B cations both assume formal 3+ valence states (as described in Chapter 3). One of the primary motivations for studying these 3:3 compounds is that cation disorder does not lead to a charge imbalance (although there will be some local charge redistribution in the vicinity of defects). It may be that the equivalence of the charge states leads to lower disorder energies; however, for many perovskites a significant cation size difference exists.

An exceptionally broad range of ABO_3 compositions is considered with the A cation radii ranging from Sc^{3+} (1.05 Å) to La^{3+} (1.34 Å) and the B cation radii ranging from Al^{3+} (0.535 Å) to In^{3+} (0.8 Å). Consequently, at one extreme of the compositional range the A and B cations are of closer in size. Such $A^{3+}B^{3+}O_3$ compositions no longer exhibit a perovskite-like structure, but are of the cubic bixbyite type. Previous work [146] considered the radiation tolerance of the bixbyite structure by investigating the rare earth oxides Er_2O_3 and Dy_2O_3. Both compounds were found to be highly radiation tolerant. Part of the explanation given for this observation was the similarity of the bixbyite and fluorite structures. Although the rare earth bixbyites are not within the present compositional range, this study also provided further insight into why bixbyite materials are radiation tolerant.

In this study, atomic scale computer simulation techniques were used to predict the structures and energies associated with defect formation in these compounds.

Those structures which exhibit larger energies for disorder processes will assume a greater residual or retained energy upon disorder and on this basis are assumed less radiation tolerant [4]. Such an approach proved successful in earlier work predicting the relative radiation tolerance of an extended set of materials with the pyrochlore structure [4]. Those conclusions were also supported by direct molecular dynamics simulations of cascades in pyrochlores [195]. It is acknowledged, however, that factors other than retained energy, in particular damage recovery or annealing processes, are important in determining the radiation tolerance of materials [176]. As such, the energies for those processes that form the defects necessary for transport processes are of interest.

4.1.3 Crystallography

Perovskite

In order to describe the intrinsic defect behaviour of perovskites, with a view to predicting the radiation tolerance, the structure predictions (Chapter 3) have been chosen for the case where the garnet decomposition reaction is negated. Therefore all compositions presented here are assumed to adopt the ABO_3 stoichiometry.

Pyrochlore

Since comparison will be made to pyrochlore compounds it is necessary to discuss the pyrochlore structure. The general formula for pyrochlore is $A_2B_2O_7$ and simple pyrochlores exist in two different forms: (3+, 4+) with formula $A_2^{3+}B_2^{4+}O_7$ and (2+, 5+) with formula $A_2^{2+}B_2^{5+}O_7$. However, for the purpose of this report, only

3+, 4+ pyrochlores were considered. The pyrochlore crystal structure has been widely investigated, both generally [196, 197] and for application to HLW storage [5, 198, 199]. The full pyrochlore unit cell contains eight formula units and has spacegroup $Fd\bar{3}m$ (227) [200]. The ion positions are presented in Table 4.1 and the full pyrochlore unit cell is shown in Figure 4.1. It is important to note that the atom positions have been specified relative to the origin at a B site.

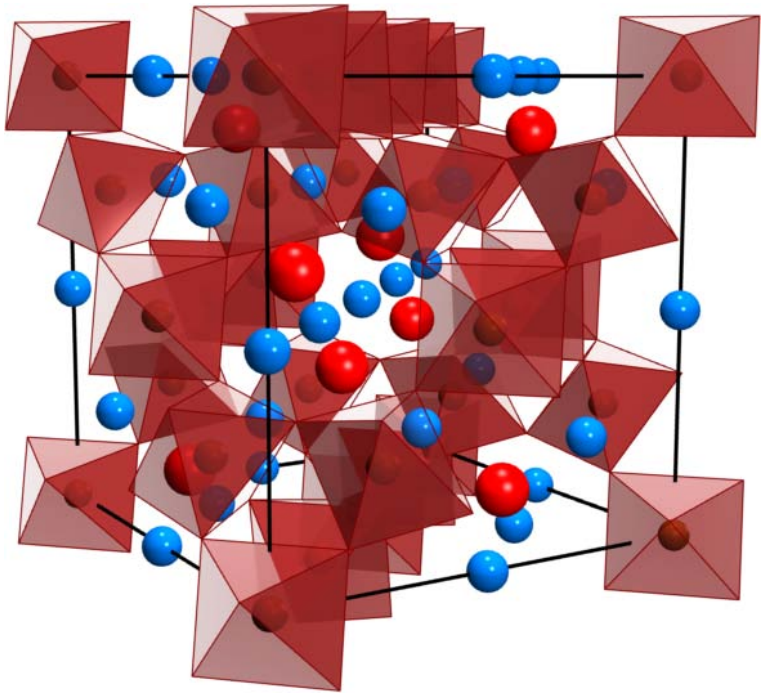

Figure 4.1: Full unit cell of pyrochlore oxide. The red octahedra represent the oxygen octahedra with oxygen ions on the vertices, the red spheres represent the 8a oxygen position and the large blue spheres represent the A^{3+} cation. The smaller B^{4+} cations are within the oxygen octahedra.

The pyrochlore structure can be considered as a defective, distorted fluorite. The general formula for the fluorite would be $(A,B)_4O_8$ compared to the pyrochlore which has one less anion, $(A_2B_2O_7)$. This oxygen vacancy causes a distortion to the surrounding oxygen ions which results in the pyrochlore structure (see Figure

Table 4.1: Atomic positions for pyrochlore oxides [150]

Site	Location	Co-ordinates
A^{3+} cation	(16d)	($\frac{5}{8}$, $\frac{5}{8}$, $\frac{5}{8}$)
B^{4+} cation	(16c)	($\frac{1}{8}$, $\frac{1}{8}$, $\frac{1}{8}$)
O(1) anion	(48f)	(x, 0, 0)
O(2) anion	(8b)	($\frac{1}{2}$, $\frac{1}{2}$, $\frac{1}{2}$)

4.1), it is noteworthy that the cations are still on fluorite sites (Table 4.1). As with the perovskite, the B cations are smaller than the A cations, and are surrounded by oxygen octahedra such that BO_6 corner sharing octahedra form sheets parallel to the (111) plane.

4.2 Results and Discussion

4.2.1 Disorder Processes

Once the lowest energy lattice structure had been identified (see Chapter 3), the individual component defect energies were calculated. Then each compound was assigned Schottky, oxygen Frenkel, cation Frenkel or antisite defect process energies by following the total defect processes described in Equations 4.1, 4.2, 4.3, 4.4 and 4.5 below. The positions of the interstitial defects necessary for Equations 4.2, 4.3 and 4.4 is given in Table 4.2.

$$A_A^X + B_B^X + 3O_O^X \rightleftharpoons V_A''' + V_B''' + 3V_O^{\bullet\bullet} + ABO_3 \tag{4.1}$$

$$O_O^X \rightleftharpoons V_O^{\bullet\bullet} + O_i'' \tag{4.2}$$

$$A_A^X \rightleftharpoons V_A''' + A_i^{\bullet\bullet\bullet} \tag{4.3}$$

$$B_B^X \rightleftharpoons V_B''' + B_i^{\bullet\bullet\bullet} \tag{4.4}$$

$$A_A^X + B_B^X \rightleftharpoons A_B^X + B_A^X \tag{4.5}$$

Table 4.2: The position of the oxygen interstitial defect as used in the oxygen Frenkel reaction (Equation 4.2).

Crystal Structure	Wyckoff Site [150]	Position
Pnma	4a	(0, 0, 0)
R$\bar{3}$c	18d	(0.5, 0, 0)
P6$_3$cm	12d	(0.875, 0.525, 0.05)
Ia3	24d	(0.25, 0.46, 0)

In a similar manner as described for perfect lattice energies, defect process energies can be represented over the full compositional range on an energy contour map. Low energy regions identify compounds for which the defect process is more favourable. In order to allow for comparison between the different defect reactions, the energies presented were normalised per defect, as dictated by a mass action analysis [201], i.e. the Schottky process has a normalisation factor of 5, whilst the antisite and Frenkel processes have normalisation factors of 2 (see Appendix A).

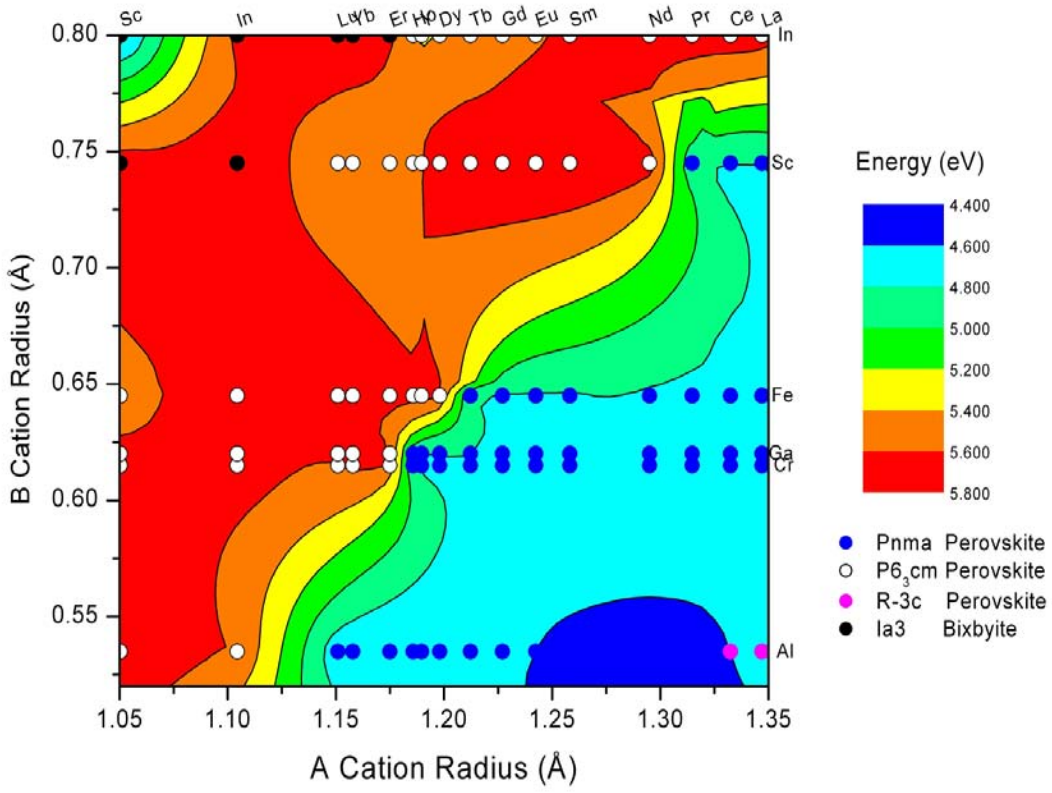

Figure 4.2: Schottky reaction energy contour map.

It can be seen from Figure 4.2 that the Schottky defect process energy (see Equation 4.1) shows considerable variation with changes in crystal structure over the compositional space. Compositions which adopt the rhombohedral ($R\bar{3}c$) and orthorhombic (Pnma) symmetries show little variation with changes in composition. As the stability of the orthorhombic phase decreases, with decreasing A^{3+} cation radii, the Schottky defect energy increases. The Schottky energy reaches a maximum of 5.7 eV for compositions which adopt the hexagonal ($P6_3cm$) symmetry. The Schottky energy then decreases for compositions which adopt the bixbyite (Ia3) symmetry.

The closer the compositions are to the classical view of the perovskite with the

corner shared octahedra, the lower the Schottky defect process energy. Within the hexagonal materials, the oxygen ions do not form octahedra, and the structure is much more open than any of the other symmetries (see Chapter 3). The more open the different ABO_3 structures, the higher the Schottky reaction energies; this is due to the higher vacancy formation energies for these materials. The closer packing of the rhombohedral and orthorhombic structures leads to lower vacancy energies since these materials are able to accommodate the extra space more readily than the hexagonal perovskite. This argument also holds true for the bixbyite materials. This is a very high symmetry structure, and here all the cation sites are surrounded by oxygen octahedra, and thus, the bixbyite structures are densely packed and they are readily able to accommodate lattice vacancies.

Figure 4.3 shows the oxygen Frenkel defect reaction energy contour map (see Equation 4.2). Perovskite compositions that exhibit the rhombohedral crystallography have the highest oxygen Frenkel defect reaction energies at 6.4 eV. The energy then decreases for those compositions adopting the orthorhombic crystallography. Moving further across Figure 4.3 (decreasing A cation radii, and increasing B cation radii), it can be seen that at the boundary between the orthorhombic and hexagonal material a step in the energy values occurs. The oxygen Frenkel reaction energies are lower for the hexagonal compositions than the other perovskite phases. The defect energies continue to decrease reaching a minimum of 3.2 eV for materials that exhibit the bixbyite structure. The general trend in the defect reaction energy for the perovskite materials shows that there is a decrease as the crystallography becomes more open. The oxygen Frenkel reaction shows competing factors, there is an energy contribution due to the formation of an oxygen vacancy, and one for the formation of an interstitial oxygen defect.

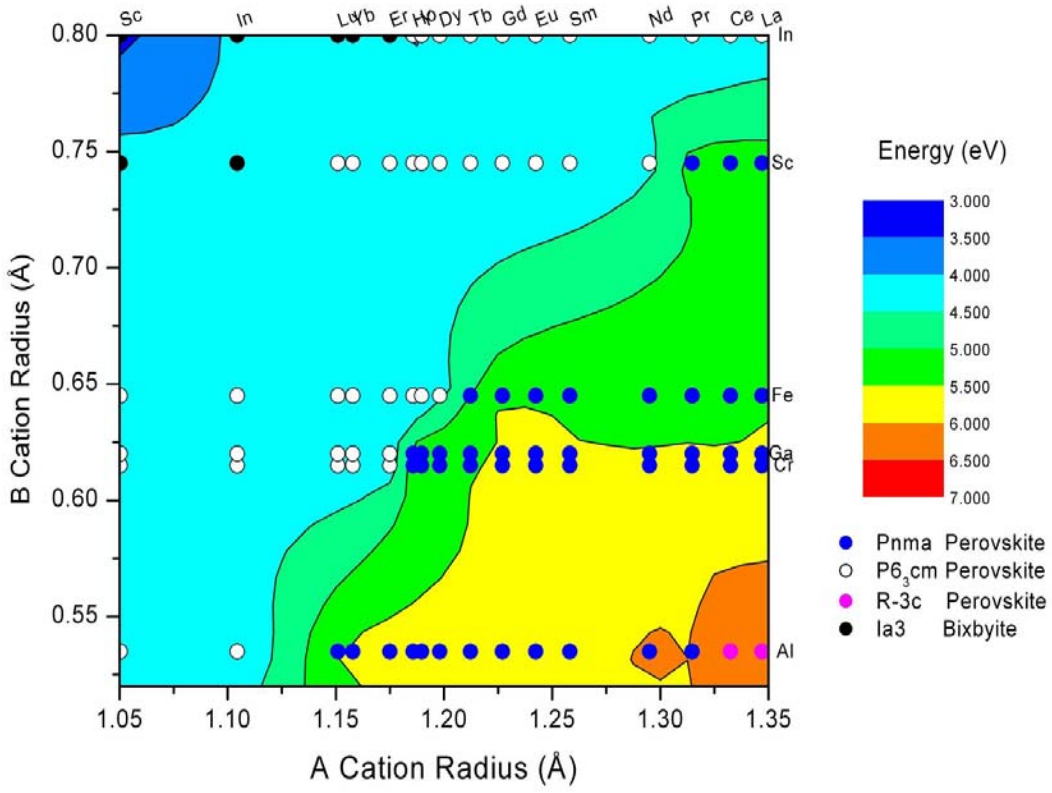

Figure 4.3: Oxygen Frenkel reaction energy contour map.

As the crystal structures become more open with the increasing distortion of the BO_6 octahedra ($R\overline{3}c$ > Pnma > $P6_3cm$) the lattice is able to accommodate the interstitial defect more readily. The bixbyite lattice is able to accommodate defects more readily again due to the nature of the lattice. Despite the fact that the bulk of the crystal structure consists of octahedra, both BO_6 and AO_6, there is a large central interstitial site which takes the form a double oxygen 6 membered ring (see Chapter 3).

The A cation Frenkel defect reaction energies (Equation 4.3) are shown in Figure 4.4. The general trend in the defect energies is similar to that for the oxygen

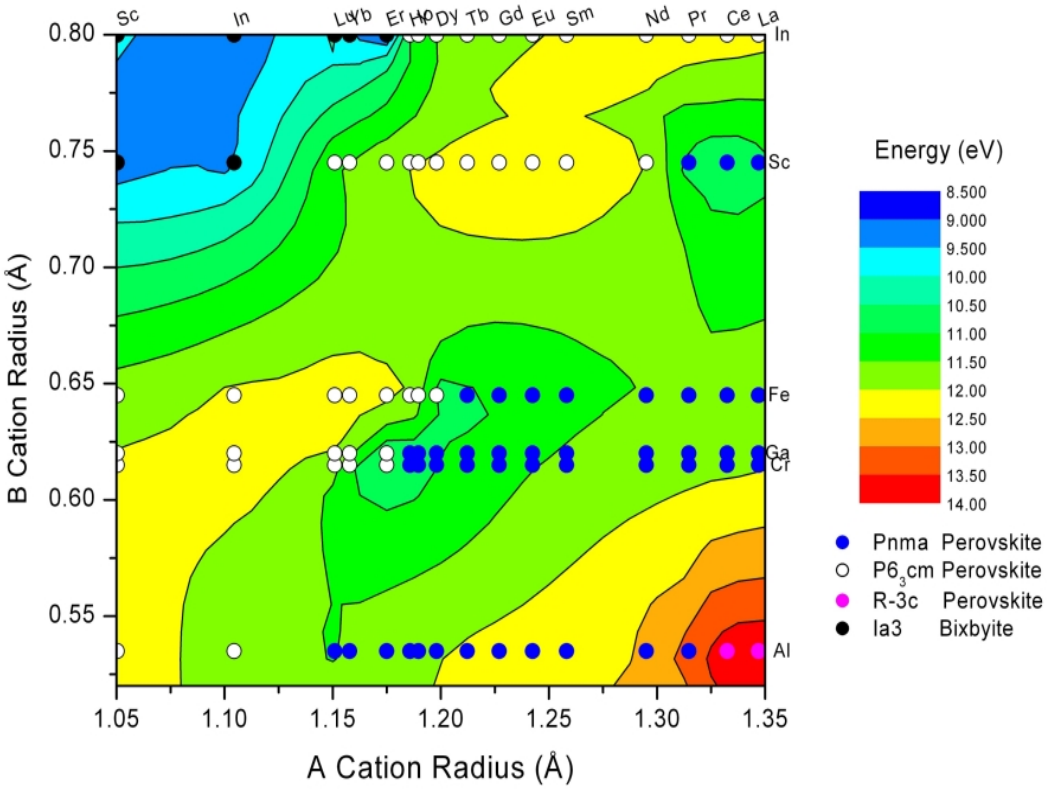

Figure 4.4: A^{3+} cation Frenkel reaction energy contour map.

Frenkel reaction energies (Figure 4.3), however the values are considerably higher, varying between 14.0 to 9.0 eV for the A cation Frenkel compared to a range of 3.2 to 6.4 eV for the oxygen Frenkel. Again the highest energy values are found for the rhombohedral perovskites. The defect energies then decrease across the orthorhombic stability region and there is somewhat of a discontinuity is seen at the boundary between the orthorhombic and hexagonal materials. The defect energy then increases slightly for these hexagonal perovskites and then drops back off for the bixbyite materials.

The reason for this energy trend is the same as that for the oxygen Frenkel reaction,

namely that the energy penalty for creating a vacancy and an interstitial defect changes with crystallography. However, since the A cation is more highly charged and larger than the oxygen anion, the lattice distortion introduced by both creating the vacancy and the interstitial defects is much larger than that for the oxygen defects, thus the higher energy obtained for the A cation Frenkel reaction component compared to the oxygen Frenkel reaction.

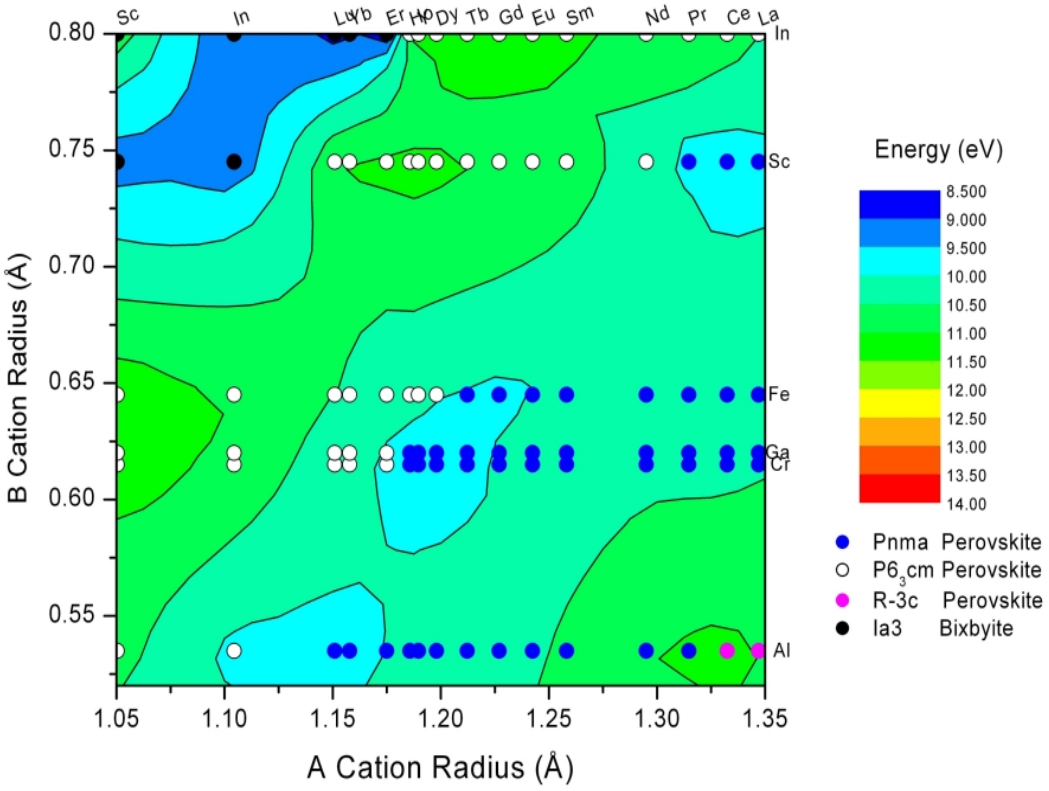

Figure 4.5: B^{3+} cation Frenkel reaction energy contour map.

The B cation Frenkel defect reaction energies (Equation 4.4) are presented in Figure 4.5. These reaction energies show considerably less variation over the compositional range than the other defect process energies, varying from a maximum of 11.0 eV

to a minimum of 9.4 eV. Here the defect energy values are intermediate to those of the oxygen Frenkel and A cation Frenkel reactions. The energy trend decreases from the rhombohedral perovskite though the orthorhombic material and reaches a minimum at the low energy boundary between the orthorhombic and hexagonal materials. The energy then increases for these hexagonal materials before decreasing again for the bixbyite compositions.

The same explanation for this trend can be made as for the oxygen and A cation Frenkel reaction energy trends, however, due to the size of the B cations being smaller than the A cations the energy values are lower due to the decreased lattice distortion created by these defects.

The observed small increases in the cation Frenkel energies (both A and B cation) for the hexagonal materials is due to the coordination of the A and B cation being lower for this structure (7 and 5 fold) than for the orthorhombic and rhombohedral perovskite structures (12 and 6 fold), thus the sizes of the cation sites are slightly smaller. The energy to create the vacancies is therefore larger due to increased lattice distortion.

The energies for the antisite defect reaction (Equation 4.5) are presented in Figure 4.6. Again, the highest energy is for the rhombohedral compositions with a value of 5.8 eV. The defect energy then decreases in a regular manner through all compositions and structures to a point where the energy is 0 eV for the bixbyite materials. A defect reaction energy of zero infers that the energy balance between the strains induced by creating the two antisite defects cancels out. This can be explained simply by consideration of the crystallography. Within the bixbyite structure each of the cation sites are octahedrally coordinated by oxygen, and as such the sites are very similar. In essence, the antisite reaction does not cause significant disorder to

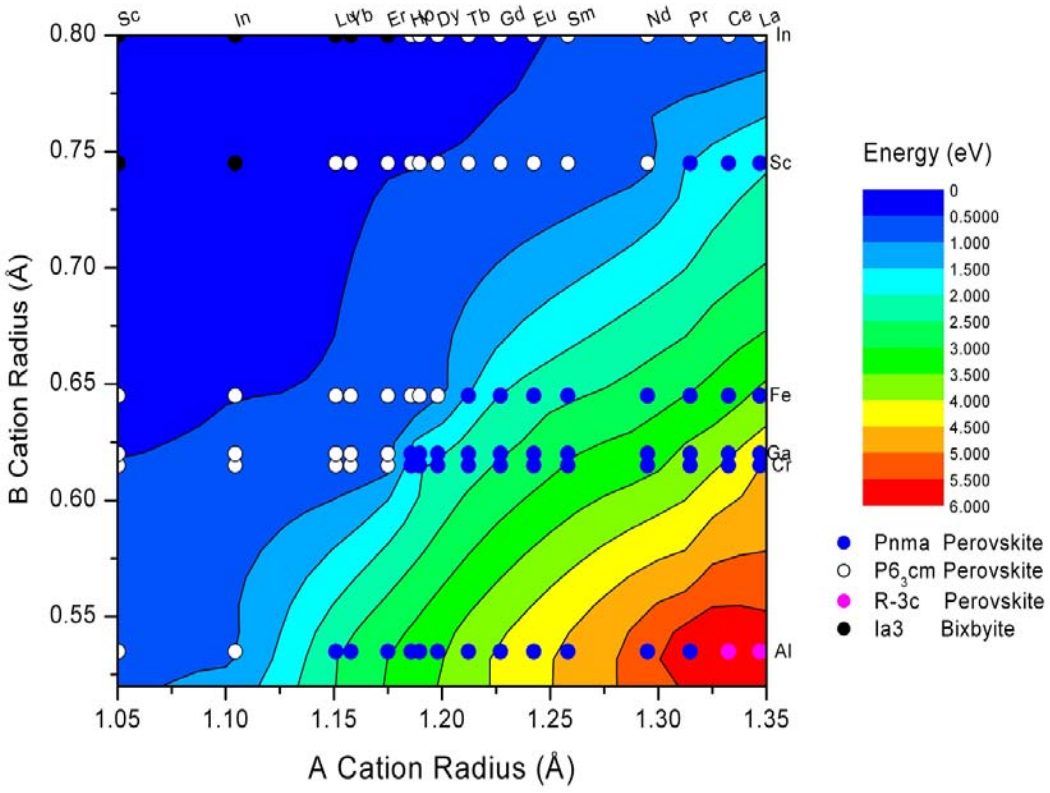

Figure 4.6: Antisite reaction energy contour map.

the lattice.

The overall trend in the antisite defect energies can be described by considering the tolerance factor (Equation 3.2). Although the tolerance factor (t) was originally derived to predict the distortion of a perovskite lattice from an idealised cubic structure, it can also be used to understand the variation exhibited by the antisite energy. This is because the tolerance factor is a relative measure of the difference in size of the A and B cations and by inference how much distortion would be necessary to accommodate an A cation at a B site and vice versa (i.e. as in the antisite reaction). In this regard, it is convenient to quantify this for the perovskite compositions

alone, such that low t values (i.e. less than 0.8) indicate that the cations fit well in opposing cation sites (i.e. an A cation on a B lattice site and vice versa), while high t values (i.e. greater than 0.8) suggest that they fit rather less well. Thus the value for a perfect cubic perovskite (i.e. 1) would imply a high antisite energy. By comparing Figures 3.9 and 4.6, it is clear that there is an excellent correlation between our calculated antisite energy and the tolerance factor.

4.2.2 Comparing Defect Processes

The Schottky, oxygen, A and B cation Frenkel and antisite reactions can be compared by considering Figures 4.2 to 4.6. It is at once apparent that the Schottky and oxygen Frenkel disorder processes show less variation in energy as a function of cation radii than the antisite process. Furthermore, the cation Frenkel reactions have much higher energies than any of the other processes. Since they are much higher in energy, the A and B cation Frenkel reactions are the least favourable processes.

The smaller predicted variation in Schottky energy as a function of cation radius is a consequence of competing factors. In the Schottky reaction (Equation 4.1) the displaced ions form new lattice and as such, the lattice energy and hence its variation with component cation radii is an important factor. This was shown in Figure 3.8 and clearly the lattice energy gain is greatest for compositions in the bottom left hand corner. The second term concerns the energy to form vacancies. Higher energies (less favourable) will result in materials with higher Madelung or electrostatic energies. Although these vary somewhat between structure types, values principally increase as the interatomic separation decreases. Thus, higher energies are expected when both the A and B cations are small, i.e. the opposite variation observed with

the lattice energy (see Figure 3.8). These electrostatic terms are therefore working in opposition, and the net effect is a smaller variation in Schottky energy as a function of cation radii. Contributions from the short range pair energies now become important. Consequently structure type boundaries where there is a change in ion coordination should show up in the Schottky energy map. In Figure 4.2, there is evidence of such a change between Pnma (VI, XII) and $P6_3cm$ (V, VII) but not $R\bar{3}c$ (VI, XII) to Pnma (VI, XII).

By comparing the results in Figures 4.2 and 4.6 it is at once evident that there is a change in lowest disorder process energy from Schottky to antisite as a function of the cation radii. If this is expressed in terms of the tolerance factor, the swap-over occurs at a t value between 0.99 and 0.98 with the antisite reaction dominant for all lower values. Thus, only in a small portion of the cation radii space (i.e. at the bottom right) does Schottky disorder dominate over antisite. Furthermore, in this region, the difference in process energies is not great, and thus materials such as $LaAlO_3$ should exhibit complex defect equilibria.

It is also possible to compare the oxygen Frenkel and antisite energies. The oxygen Frenkel energy decreases somewhat as the A cation radius increases and the B cation radius decreases, in a similar manner to the antisite process energies. Although this decreases to a value considerably below the Schottky for a majority of the compositional range, the oxygen Frenkel energy does not decrease to the same extent as the antisite and is never the dominant defect process. Again some evidence of the Pnma to $P6_3cm$ structure change is seen (Figure 4.3).

4.2.3 Implications for Radiation Tolerance

The intrinsic defect processes all effect the radiation tolerance of the ABO_3 compositions. However, predictions of the radiation tolerance that rely solely on the intrinsic defect processes are based on the retained defect process energy argument. This assumes that the greatest contribution to the retained energy upon irradiation is due to the dominant defect process (i.e. lowest energy). In this case, the tolerance of the materials essentially follows the antisite results in Figure 4.6 and radiation tolerance follows structure type in the order $R\overline{3}c < Pnma < P6_3cm < Ia3$. Clearly the perovskite-like structures are significantly less tolerant than bixbyite, although there is considerable variation between the three structures $R\overline{3}c$, Pnma and $P6_3cm$.

There is, however, an inherent limitation with this analysis. The antisite reaction only results in the formation of substitutional defects; no vacancy or interstitial defects are involved. Of course, not only will other types of defects form through radiation damage, but, as previously mentioned (Section 4.1.2), it is these latter types of defects that are necessary to help anneal damage through transport mechanisms. Since the recovery will take place with minimal external energy input unlike the high energy damage processes, it is more important to consider the oxygen sublattice, because in ceramics the anions are far more mobile than the cations. Thus, for damage evaluation and recovery, it would seem that the relative Schottky or oxygen Frenkel energies provide a valuable criteria for differentiating between compositions. If this is correct, the recovery process of all the perovskites would be similar (since the combined lowest energies in Figures 4.2 and 4.3 are almost constant as a function of radii). In this way, the main criterion for the tolerance assessment, at least when isolated defects are considered, should be the retained energy of the lattice. However, all perovskites would still be considerably less tolerant than the bixbyites.

4.2.4 Comparison to Pyrochlore/Fluorite

The perovskite defect process energies can be compared to the equivalent lowest energy defect process energies for other materials. Here, comparison is made to the fluorite and pyrochlore oxides investigated previously [4, 5]. In this case, the antisite energies of the perovskites are well above those for the zirconium containing pyrochlore/fluorite materials (e.g. $Er_2Zr_2O_7$ (0.6 eV) and $Gd_2Zr_2O_7$ (1.8 eV) [4]). As such, only selected $P6_3cm$ perovskites could be as impressively radiation tolerant as the best zirconate pyrochlores. On the other hand, the titanate pyrochlores exhibit antisite defect energies of typically 2.9 eV which is equivalent to the lowest energy for the Pnma perovskites. On this basis alone, only the most radiation tolerant Pnma perovskites would approach the tolerance of the least tolerant titanate pyrochlores. Conversely, the bixbyite materials should show excellent radiation tolerance.

The oxygen Frenkel defect energies for the perovskites (Figure 4.3) are higher than those for the pyrochlores. For example, the zirconate pyrochlores $Er_2Zr_2O_7$ and $Gd_2Zr_2O_7$ exhibit oxygen Frenkel energies of 2.5 eV and 2.0 eV respectively [5], both being lower than corresponding results for the perovskite materials. However, the titanate pyrochlores have values that are similar to the Pnma perovskites, for example, $Gd_2Ti_2O_7$ has an oxygen Frenkel energy of 5.6 eV [5]. Consequently, values for the bixbyites, which are as low as 3.0 eV, compare favorably to the titanate pyrochlores and are not significantly higher than the zirconates. On this basis the bixbyites are again predicted to be highly radiation tolerant.

Up to this point, a model has been suggested that requires antisite and oxygen Frenkel lattice defects. However, the stability of such defects depends not only on their individual energies, but also on the interactions between them. This is charac-

terised by the reduction in formation energy when the defects are associated (known as the binding energy). The work on pyrochlores considered the representative defect cluster $\{A_B^X : B_A^X : V_O^{\bullet\bullet} : O_i''\}^X$, a combination of antisite and oxygen Frenkel reactions where the defects are in their nearest neighbour positions [5].

Table 4.3: Comparison of the total defect energies for isolated defects and clusters $\{A_B^X : B_A^X\}^X$ for different compositions of perovskite and pyrochlore oxides. Note: the energies presented in this table have not been normalised. * composition is not stable as perovskite and irradiation may cause decomposition to garnet.

	Total Defect Energy (eV)	
	$\{A_B^X : B_A^X\}^X$	
	Isolated	**Clustered**
Perovskite		
$GdAlO_3$	8.20	7.05
$LaAlO_3$	11.98	10.59
$GdFeO_3$*	4.24	4.03
$LaFeO_3$	7.44	6.30
Pyrochlore	[5]	
$Gd_2Ti_2O_7$	6.09	4.98
$La_2Ti_2O_7$	5.94	4.59
$Gd_2Zr_2O_7$	3.68	2.86
$La_2Zr_2O_7$	4.52	3.45

Interestingly, when different geometries of this cluster were investigated for pyrochlore, the oxygen Frenkel component sometimes self annihilated in the presence of the cation antisite pair (yet, when the oxygen Frenkel pair are alone, they do not annihilate). Thus in Table 4.3 for these pyrochlores the energy for the $\{A_B^X : B_A^X : V_O^{\bullet\bullet} : O_i''\}^X$ cluster are the same as for the clustered antisite pair, $\{A_B^X : B_A^X\}^X$. Such behaviour was not observed in equivalent perovskite clusters. This may in itself be a significant difference between pyrochlores and perovskites

in regard to their ability to tolerate radiation damage through damage annealing. Nevertheless, in order to compare equivalent defect clusters, energy comparisons were made for adjacent antisite pairs $\{A_B^X : B_A^X\}^X$ (see Table 4.3 for examples). It is possible to fix the defects at the clustered lattice positions, however this then is forcing an outcome for the lattice relaxation and in this case comparison would not be reliable. Critically, for perovskites the values when the defects are associated (i.e. clustered) are only modestly less than when the defects are isolated. Conversely, in pyrochlore materials, cluster formation values are considerably less than for isolated defects (Table 4.3). The larger binding energy for pyrochlores means that a significant difference between the antisite energy for $GdFeO_3$ compared to lower zirconate pyrochlore values can now be seen. The other perovskites maintain their higher defect process energies.

Clearly, for the pyrochlore materials these antisite defects are more strongly bound than for the perovskite materials. This may imply that in perovskites, as the defect concentrations increase, i.e. with damage accumulation, the retained energy increases more quickly. On this basis, all the perovskites should be significantly less radiation tolerant than pyrochlores. However, it would be appropriate to apply further analysis such as molecular dynamics (because of the great number of cluster configurations) before this can be stated with confidence.

4.3 Conclusion

By relating the energies for defect processes to radiation tolerance, predictions of how the radiation tolerance varies across an extensive series of $A^{3+}B^{3+}O_3$ compositions is possible. In this regard the intrinsic defect processes are dominated by

the antisite reaction. Certainly cation disorder is expected to be a consequence of radiation damage and as such, this is an important reaction as it is one measure of retained energy. However, damage can recover or anneal only if defects are present to mediate ion transport. Consequently, the lowest energy for either oxygen Frenkel or Schottky disorder must be considered concurrent with cation disorder. On the basis of these three reactions, the order for radiation tolerance between compositions roughly follows the perovskite tolerance factor (see Equation 3.2 and Figure 3.9). In terms of the ABO_3 crystal structure, this means that the predicted order of increasing tolerance is $R\overline{3}c < Pnma < P6_3cm < Ia3$, where $R\overline{3}c$ and Pnma are "true" perovskites and Ia3 is bixbyite. Only the formation energies for defects involved in ion transport have been calculated. Therefore, in future work, it would be valuable to construct a map for anion (and possibly cation) migration activation energies equivalent to the work on pyrochlores [28, 202].

By comparing the equivalent defects in $A_2B_2O_7$ pyrochlore oxides with previous simulations [4, 5], the relative tolerance of ABO_3 oxides can be assessed. Based on the results for isolated defects, none of the perovskites would be expected to exhibit the exceptional radiation tolerance of the zirconate or cerate pyrochlores/fluorites, i.e. $A_2Zr_2O_7$ or $A_2Ce_2O_7$ [4, 146] (the Ia3 bixbyites will be treated separately). However, the best perovskites would have a similar tolerance to the intermediate titanate pyrochlores $A_2Ti_2O_7$. When the reaction energies based on clustered defects are considered (Table 4.3), again the perovskite materials appear less tolerant than the zirconate pyrochlores.

A low energy for the antisite defect process in itself, is not sufficient for a radiation tolerant material. For the bixbyite materials, however, the oxygen Frenkel energy is similar to the oxygen Frenkel of pyrochlores. It is important to note that formation of

lattice defects is only part of the consideration of the tolerance of a material, and that the ease at which the material anneals such damage will be a major contribution. As such the energy associated with transport and the activation energy for ion migration are also significant.

Clearly, the low defect formation energies exhibited by the bixbyite oxides are consistent with these materials being approximately as radiation tolerant as the better pyrochlores. It seems logical to assume that this is in part a consequence of the similarity between the bixbyite and fluorite structures [146]. Furthermore, at higher damage, this similarity means that the bixbyite structure may be able to assume the lower symmetry disordered fluorite structure, which has been shown previously to be highly radiation tolerant [146].

It is also possible that upon irradiation, materials that lie on the cusp of the hexagonal to bixbyite boundary can also assume the cubic bixbyite (or disordered fluorite structure) since the differences in lattice energies are small. In such a case those compositions would become more radiation tolerant than in their original $P6_3cm$ phase. This may provide an interesting avenue for experimental investigation.

Finally, returning to the question originally posed in the introduction (Section 4.1.2): does the equivalence of charge between A^{3+} and B^{3+} cations in the perovskite systems imply that they show some significant degree of radiation tolerance? On the basis of this approach, the answer appears to be negative. For the $R\overline{3}c$ and Pnma (i.e. the "true" perovskites), the difference in ion size and the associated crystallography means that these materials should not be highly radiation tolerant due to the inherent lattice strains introduced upon disorder. Conversely, materials with the bixbyite structure should show considerable tolerance.

The defect energy results presented here suggest that there will be no $A^{3+}B^{3+}O_3$ perovskites as radiation tolerant as the $A_2Zr_2O_7$ zirconate pyrochlore/fluorite related compounds previously investigated [4]. The experimental data thus far are in agreement with predictions, whereby ion doses that cause amorphisation in $Er_2Ti_2O_7$ but not $Er_2Zr_2O_7$ also cause amorphisation in all the $A^{3+}B^{3+}O_3$ perovskites considered. Clearly the perovskites are not as tolerant to ion irradiation as the best fluorite related materials. Further experimental work will be needed to validate the predicted order of perovskite radiation tolerance which should be rather distinct. As such it would be interesting to reduce the ion irradiation flux to see if it is possible to differentiate between the various perovskites.